6(2009) 301 – 321

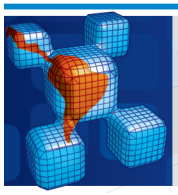

Latin American Journal of Solids and Structures
www.lajss.org

Fractomechanics parameter calculus using the Discrete Element Method with bars

Abstract

The calculus of fractomechanic parameters using computational numerical methods is still an active area of investigation. Traditionally, the most employed methods are the Finite Element Method (FEM) and the Boundary Element Method (BEM). The Discrete Element Method (DEM) with bars is another alternative, although its usage is not so extended in the solid mechanic area. DEM success in the simulation of failure mechanisms and defect nucleation motivates its implementation in fracture mechanic problems. In order to explore its potentialities in this kind of problems, this work presents the static and dynamic calculus of fractomechanic parameters of a modeled plate with DEM. For this purpose the numerical methodologies used are the same as the ones employed in the traditional numerical methods, such as FEM and BEM, as well. The obtained results, compared with the numerical and analytical results published by other authors, allow the validation of DEM for such applications where the fracture process must be doubtlessly taken into account.

Keywords

Energy release rate, J integral, stress intensity factor, fracture mechanics.

Luis Kosteski[a,*], **Ricardo Barrios D'ambra**[b] **and Ignacio Iturrioz**[a]

[a] Pos-graduate Engeneering Mechanics Program (PROMEC) of the Rio Grande do Sul Federal University (UFRGS) – Brazil
[b] Departament of Applied Mechanics – Engeneering School of the National Nordeast University – Argentine

Received 6 Apr 2009;
In revised form 27 Nov 2009

* Author email: luiskosteski@hotmail.com

1 INTRODUCTION

The calculus of fractomechanic parameters using computational numerical methods is still an active area of investigation. One of its technological applications leads to the analysis of complex geometries and boundary conditions, which, in many cases, is impossible to solve using the available solutions found in manuals [28]. No doubt that the most extended computational techniques in this area are the Finite Element Method (FEM) and the Boundary Element Method (BEM) [2], but there are new methods and techniques developed for the analysis of specific problems and applications.

In this context it is also of particular interest to count with tools capable of modeling the unstable crack propagation when the value of associated fractomechanic parameters exceed their critical values. This phenomenon is traditionally modeled using FEM and BEM based

on the cohesive surfaces methodology as in the work proposed by Needelman [22] and Aliabadi and Saleh [3], as well as discrete particular models as in works of Cundall and Hart [8], Munjiza et al. [21], Brara et al. [6].

As an antecedent of the present approach it is important to mention the pioneer work of Hrenikoff [15] who proposed to represent the continuum medium through an array of bars with an equivalent stiffness. More recently Absi [1] developed the same idea carrying out applications also using a bar arrays of equivalent stiffness to represent an elastic base foundations and the structural walls in tall buildings. It is also important to point out the works accomplished by Cundall [9] that represent the continuum through other kinds of discrete elements to simulate the mechanic behavior of granular soils in geotechnical problems.

The Discrete Element Method (DEM) with bars used in the present work, has been employed in civil and soil engineering field, applications can be found in Riera and Iturrioz [25, 26] (simulation of the behavior of shells subjected to impulsive loading), Schnaid et al., [29] (fracture in solid cement foundations on soft sand bed), Dalguer et al., [10] (recreation of the generation and subsequent spread of an earthquake) and in Rios and Riera [27] (study of the scale effect in concrete), and more recently in Miguel et al. [20] (in the rock mechanics behavior).

The success of DEM for modeling failure mechanisms in these fields and its ability to model defect nucleation motivate their application on problems of fracture mechanics. Thus, in this work the application of DEM is presented for calculating static and dynamic fractomechanic parameters in linear elastic fracture mechanic (LEFM) using usual methodologies employed in classical methods like FEM and BEM. We compare the results with those from the technical literature. The DEM capacity for capturing the critical situation is also illustrated when the fractomechanic parameters exceed the toughness of the material. Finally, there is a discussion about the performance of the employed techniques for measuring fractomechanic parameters within the context of DEM.

2 THE DISCRETE ELEMENT METHOD

2.1 Basic formulation of the method

The DEM, in the used version, primarily consists of continuous spatial discretization in reticulated regular modules, where the stiffness of bars is defined in such a way to represent the equivalent continuum. The model mass is discretized and concentrated in the model nodes. Figure 1 shows a module with eight nodes in their vertices and a central node. Each node has three associate degrees of freedom given by the spatial components of the displacement field u. Longitudinal and diagonal elements with length L_c and $\sqrt{3}/2\ L_c$ respectively join the masses. In the linear elasticity field Hayashi [14] checks the equivalence between the cubic arrangement and elastic orthotropic solid with the main axes of the material oriented in the longitudinal element direction. A restriction should be imposed in the Poisson's ratio of $\nu = 0.25$ for perfect equivalence. For other ν values there are slight differences in the shear terms, which can be ignored, especially when our interest is the nonlinear response of the studied model.

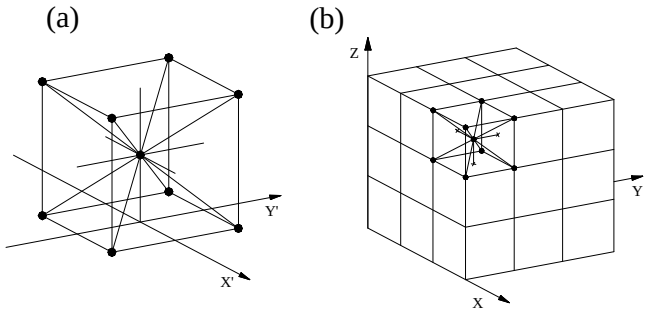

Figure 1 a) Core cubic module detail, b) Prism composed of several cubic modules.

When the materials have linear elastic behavior we can express the N degrees of freedom system motion equation resulting from the spatial discretization as:

$$\mathbf{M} \cdot \ddot{\mathbf{u}} + \mathrm{K} \cdot \mathbf{u} = \mathbf{q}(\mathbf{t}) \tag{1}$$

where $\mathbf{M}$ denotes the diagonal mass matrix, $\mathbf{u}$ and $\ddot{\mathbf{u}}$ represent displacement and generalized acceleration vectors respectively. On the other hand the vector $\mathbf{q}(\mathrm{t})$ contains the applied external forces. System (1) can be numerically integrated in time domain using a classic scheme of explicit integration (Method of Central Finite Differences).

It is important to mention that, for the present applications using an implicit integration would be more adequate, but the calculus of the fracture mechanic parameter through the present version of DEM is only a way to show the consistency of the present approach. Our main focus is in modeling critical crack propagation problems because, in this application field, the present method shows itself competitive when compared with more classic methods (FEM and BEM), and in the last case an explicit integration approach is undoubtedly the best option to integrate the motion equation in the time domain.

In the context of DEM there is a way to simulate the fracture and fragmentation of the model. In this case the constitutive law of the bar has a bilinear shape as presented in Figure 2 where G_f is associated with the toughness of the material and ε_p is a critical deformation. This characteristic allows to simulate an unstable crack propagation in a natural way. The proposed law permits to accomplish a balancing energy during the simulated problem. In the present paper this characteristic is not used, just an intensity factor coefficient is applied in subcritical situation. Documented information, about how to simulate fracture with DEM, is possible to be found in the cited works [10, 20, 25–27, 29].

3 THE FRACTOMECHANICS PARAMETER CALCULUS

Several methods to calculate the Stress Intensity Factor (SIF), not only for the static but also to the dynamic cases, are known. An excellent recompilation of them is possible to be found in Aliabadi and Rooke [2].

As it follows, the SIF calculus is presented through the expressions of Irwin of the crack

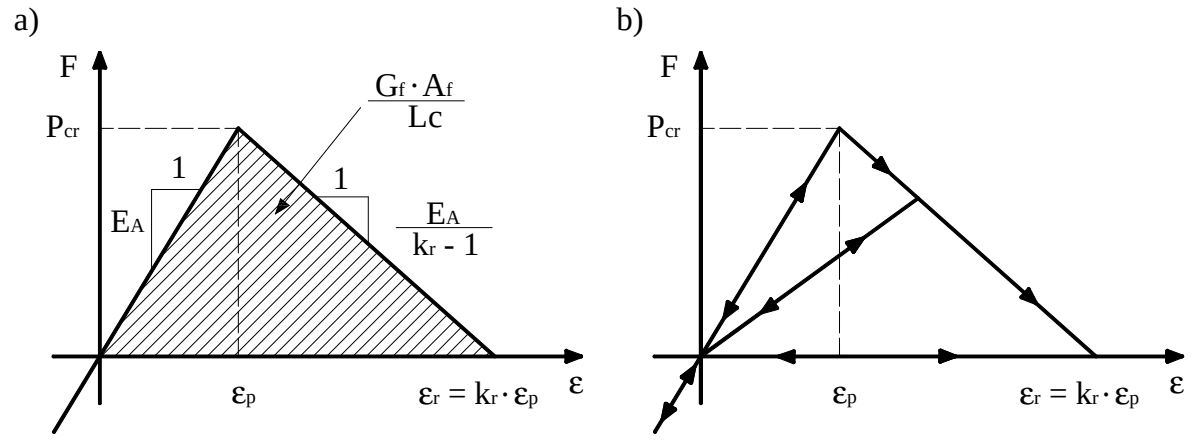

Figure 2 Reticulated bars elemental constitutive relationship – a) Adopted constitutive diagram with their control parameters; b) Loading-unloading scheme.

opening displacement expressions (COD) in the way presented by Aliabadi and Rooke [2]. Other ways of SIF calculus into DEM context are published in Kosteski et al. [18].

3.1 The SIF extrapolation calculated from COD expression.

It is possible to obtain the SIF values from the expressions supplied by Irwin and William as it is presented in [2]. In equation (2) such expression is shown.

$$K = \delta \frac{E}{4+4\nu}\sqrt{\frac{2\pi}{r}} \cdot \left(\frac{1+\nu}{2}\right) = \delta \frac{E}{8}\sqrt{\frac{2\pi}{r}} \tag{2}$$

In (2) r represents the distance between the crack tip and the point where the δ displacement is measured, as it is shown in Figure 3.

Concerning how to take the displacement δ between two points, originally in the same position but in opposite lips of the crack, it is possible to obtain:

$$K_I = v_y \frac{E}{8}\sqrt{\frac{2\pi}{r}} \tag{3a}$$

$$K_{II} = v_x \frac{E}{8}\sqrt{\frac{2\pi}{r}} \tag{3b}$$

$$K_{III} = v_z \frac{E}{8}\sqrt{\frac{2\pi}{r}} \tag{3c}$$

Where v_x, v_y and v_z are the correspondent displacements with the three modes of fracture known (mode I, II and III). In a problem where a mode of fracture I is activated as illustrated in Figure 3, taking into account the axis system indicated in this figure, we can substitute into equation (3a) v_y by δ, obtaining expression (2).

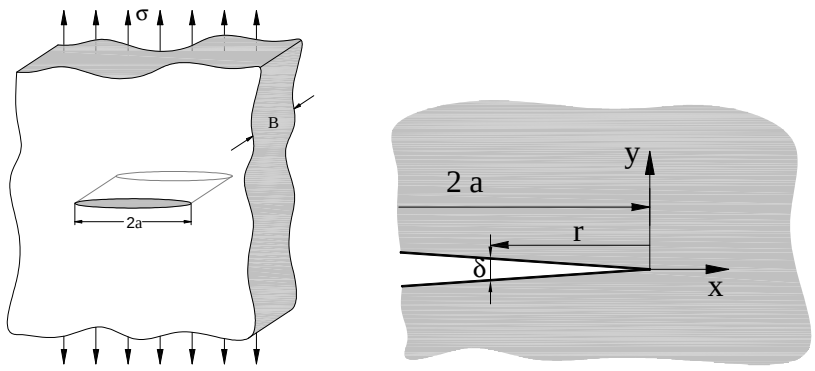

Figure 3 (a) Tensioned plate with a central crack, (b) Reference scheme for value of r and δ.

In DEM implementation, the relative displacement $\delta(r)$ indicated in Figure 3 is measured at different distances r_i near the crack tip. The stress intensity factor is calculated in each point using the expression (3a), and an extrapolation when distance r tends to zero. In this way it is possible to liberate the value of stress intensity factor from the adopted discretization. With the mentioned extrapolation, we can foresee the value for $r = 0$ through a lineal regression and with an adjustment of square minimums obtained from known data.

As COD is a local parameter, like K is, if the analyzed problem is dynamic, the elastic tension waves are implicitly taken into account. Due to this fact, the expressions (2) and (3) for static and dynamic problems are the same and that is a great advantage.

Many authors have measured the static or dynamic K using the COD as a parameter, they have used a formula that is similar to the one here shown, and among them we can mention Fedelinski et al. [12] who present the dual version of the boundary element method, Wen et al. [32], who use another version of the dual boundary element method, Tabiei and Wu [30] who work with a finite element commercial package DYNA3D.

This way to determine SIF is also cited by Nishioka [24], Aliabadi and Rooke [2] and Anderson [4].

4 THE SIF DETERMINATION: APPLICATION EXAMPLES

Results are presented after calculating the static and dynamic SIF, through the COD, as it was previously commented, implemented in DEM. Different configurations in 2 and 3D are analyzed and the results compared with the ones found in technical bibliography.

Notice that in the examples here shown there were only calculated the static or dynamic SIF, without reaching the critical situation. For this reason in all the illustrated examples high values were considered for critical strain ε_p and toughness G_f, to avoid the damage of the bar that compounds the analyzed models.

But as it was cited in the introduction and illustrated in previous work among others [10, 20, 27, 29], the fracture and fragmentation of the model is very simple to be implemented in DEM context and this characteristic is the main advantage of these method.

So the examples here presented have as a goal, that is, to show that DEM simulates correctly the behaviors foreseen by the Linear Elastic Fracture Mechanics.

4.1 Example 1: Static SIF calculus of circular discontinuity embedded in a large prismatic block

The SIF value for a circular crack embedded in a large prismatic block, which is submitted to remote tensile stress applied perpendicularly, is shown in Figure 4.a.

This case has a close solution available in the fracture mechanic classical literature [4] according to the expression bellow:

$$K_I = \frac{2}{\pi}\sigma\sqrt{\pi \cdot a} \tag{4}$$

The value obtained with (4) will be considered the reference to the DEM results (K_0) shown as follows. So, for the first example in 3D, the normalized SIF for the case studied will be equal to unity, since:

$$\frac{K_I}{K_0} = 1 \tag{5}$$

4.1.1 DEM Model

The block was modeled with a discretization of 30 elemental cubic modules in each side, the circular crack has 5 elemental cubic modules of radius as it is possible to appreciated in Figure 4.b). The total number of degree of freedom (dof) of this model is 170373 (3 dof per node).

In the same figure, the boundary conditions and the detail of node duplication are also shown in order to improve the crack model, as explained in [18].

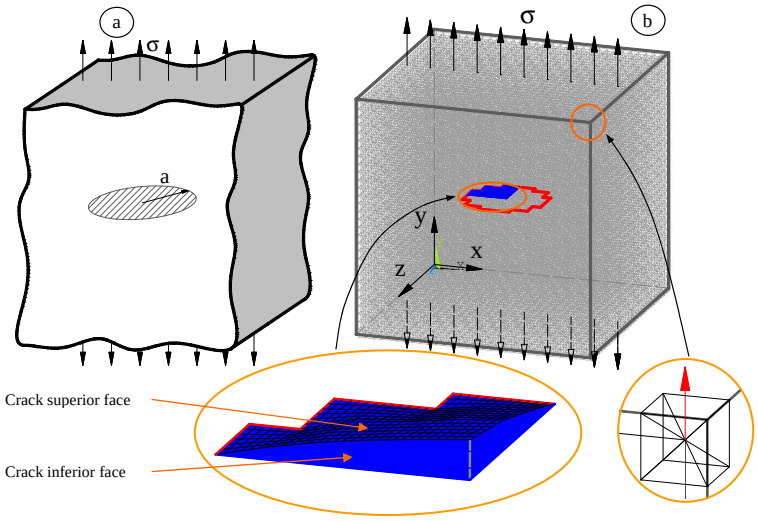

Figure 4 Example of application 1 (a) A circle plane crack embedded in a large prismatic block submitted to remote tensile stress perpendicularly to its plane. (b) DEM model where the shape of the crack is indicated, how it was modeled and how the stress was applied.

Table 1 Material properties for the studied example, and the parameter used in the simulations.

Material properties		DEM Parameters	
E	2100 MPa	Lc	3.00 E^{-4} m
ν	0.25	ν	0.25
ρ	908 kg/m^3	Δt	1.0 E^{-8} seg

4.1.2 Obtained results

In Figure 5 the obtained results observed, fluctuated around the theoretical value, taken as reference. These fluctuations appear because the model is solved in the time domain. It is possible to reduce the oscillations applying the mechanical boundary conditions (MBC) in a lower velocity.

The amplitude of this fluctuation can be minimized through a reduction of MBC velocity application or increasing the damping of the system.

The influence of the discretization was treated in other works as cited above: In Iturrioz et al. [16] the convergence analysis was performed in a rock block case submitted to pure shear load; In Tech et al [31] the convergence analysis was accomplished in a 2D example where a FIT vs. crack length was computed.

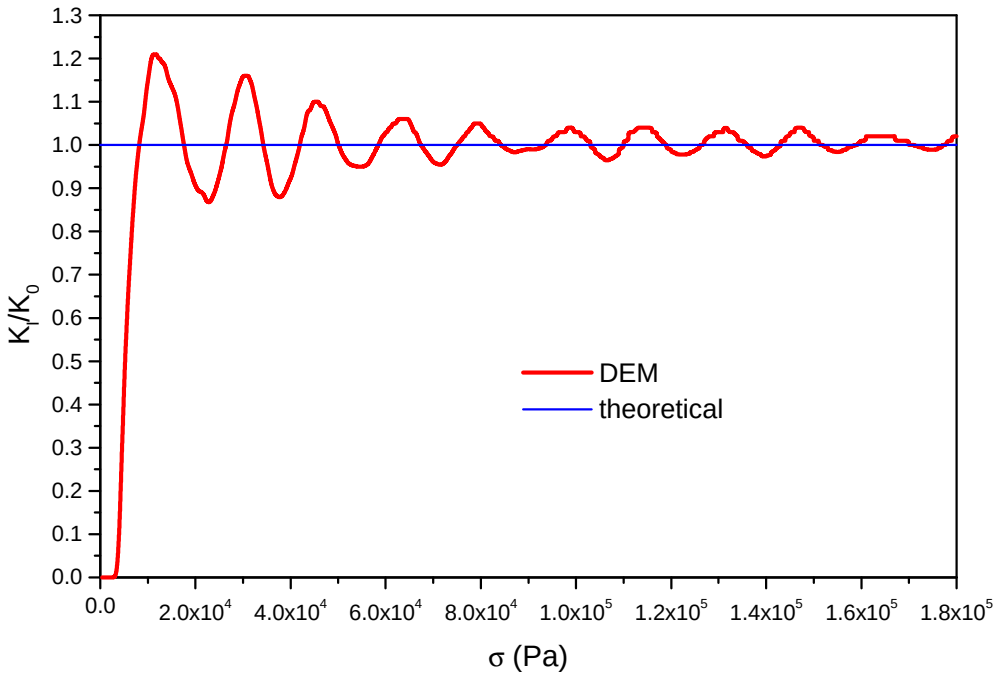

Figure 5 Results in terms of normalized SIF for the Example 1.

In the present work a convergence study was performed in one of the examples shown (see

item 4.3), where the invariance of the results for different levels of discretization in terms of dynamical SIF parameter is illustrated.

In Figures 6 (a) and (b) the vertical stress (σ_{yy}) is possible to be observed for the two cuts carried out in the block; the first one is perpendicular to the crack plane, which passes through the middle of the block, the second one passes through the crack plane.

In the second cut, perturbations can be observed in the stress values near the crack. These perturbations are associated with the level of discretization used.

It is very important to remember that the DEM primary unknowns are the displacement and nodal forces. These unknowns are associated with the discontinuing nature of the model.

The equivalent stress or strain can be obtained with a post-process routine computing the result nodal forces associated to each elemental cubic module. Details about how to compute the stress through elementary cubic modules are documented in [5].

4.2 Example 2: Static K for an elliptical plane crack embedded in a large prismatic block

The SIF for the case of elliptical plane crack embedded in a large prismatic block also has a theoretical solution [4].

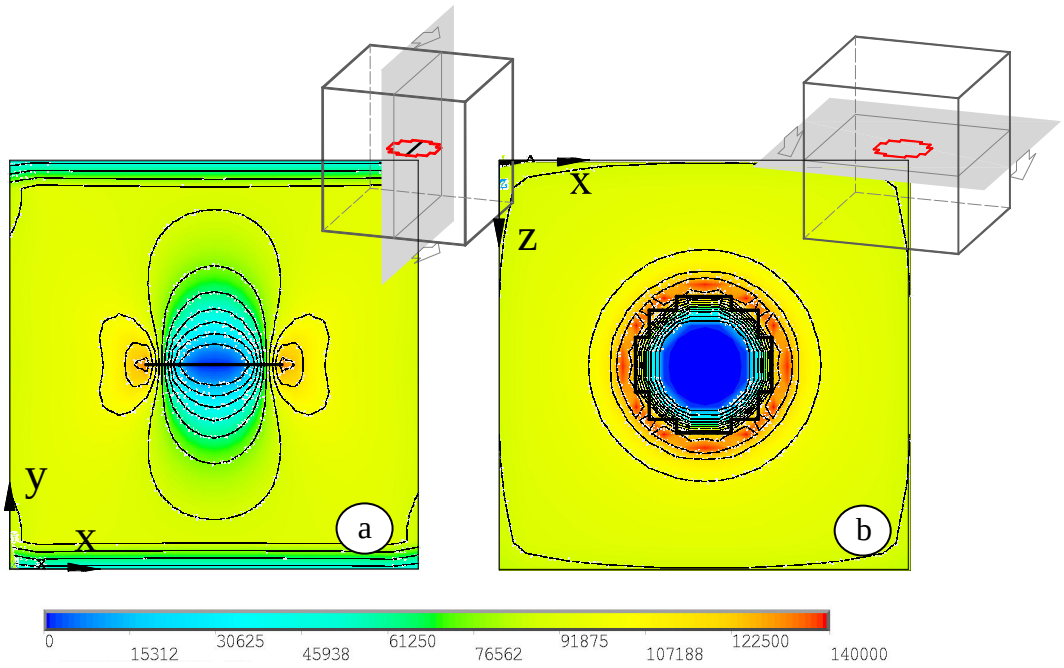

Figure 6 (a) Perpendicular cut and (b) the crack plane cut . In both cases the vertical stress was mapped σ_{yy} (Pa).

In Figures 7(a) and (b) the iso-stress surfaces are illustrated and they show a 3D stress distribution image near the crack border. Figure 7 (b) shows the iso-stress into the yellow iso-stress surface, shown in Figure 7(a).

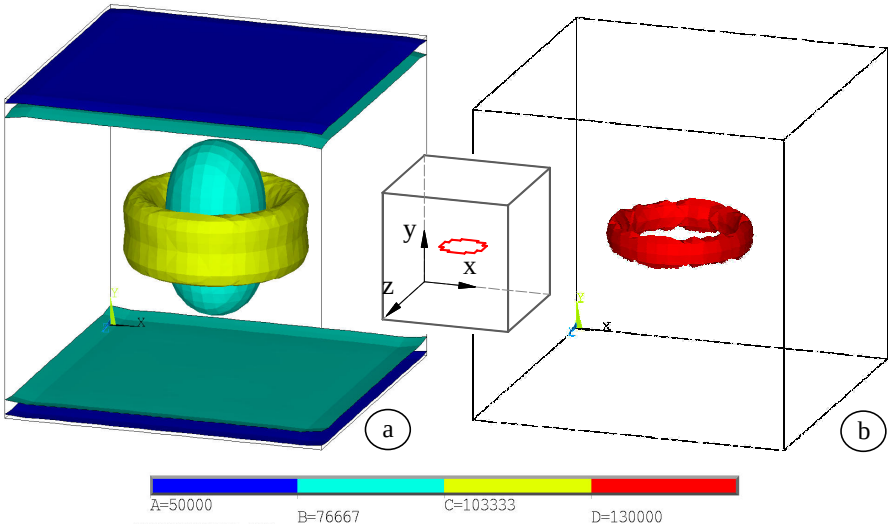

Figure 7 Scheme of the iso-stress surface σ_{yy} (Pa). Figure (b) shows the red iso-stress surface into the yellow iso-stress one shown in (a).

4.2.1 DEM Model

The DEM model of example 2 was discretized with 30 elemental cubic modules in the width (2W), the same quantities of cubic modules in the height and 15 modules in the thickness (t). The crack was discretized with 10 modules in the mayor axis (c) and 7 modules in minor axis (a). In the present case the total dof is 88116, (taken into account that the fissure nodes are double nodes).

The SIF in the minor axis direction ($\theta = 90°$) was calculated.

The boundary conditions are shown in Figure 8, a uniform tensile was prescribed in the superior side of the block and all displacements were fixed in the inferior side of the block. The tensile stress was applied with a low velocity to minimize the inertial effects in the results and, in this way, the obtained result can be considered as static. The material properties of the example modeled are the same as in example 1, see table 1.

Figure 8 indicates the geometric characteristic of example 2.

Using a classical expression shown in the bibliography [4] the result of example 2 is presented in (6), in a dimensional way. The reference used to normalize the results was given in the expression (4) (SIF for the plane circular crack embedded in a large block).

$$\frac{K_I}{K_0}^{\phi=90^o} = 1.549 \tag{6}$$

4.2.2 Obtained results

Using the COD and measuring the displacement in a coincident plane with the ellipse minor axis, the results obtained are shown in Figure 9. In this Figure it is possible to observe a good correlation between the obtained values with DEM and the theoretical value illustrated in (6).

In Figure 10 a frontal view (a) and two cuts (b) and (c) are shown, perpendicular to the crack plane, and coincident to the crack plane respectively. In this figure it is possible to observe the distribution of the vertical stress and the stress concentration generated in the crack border.

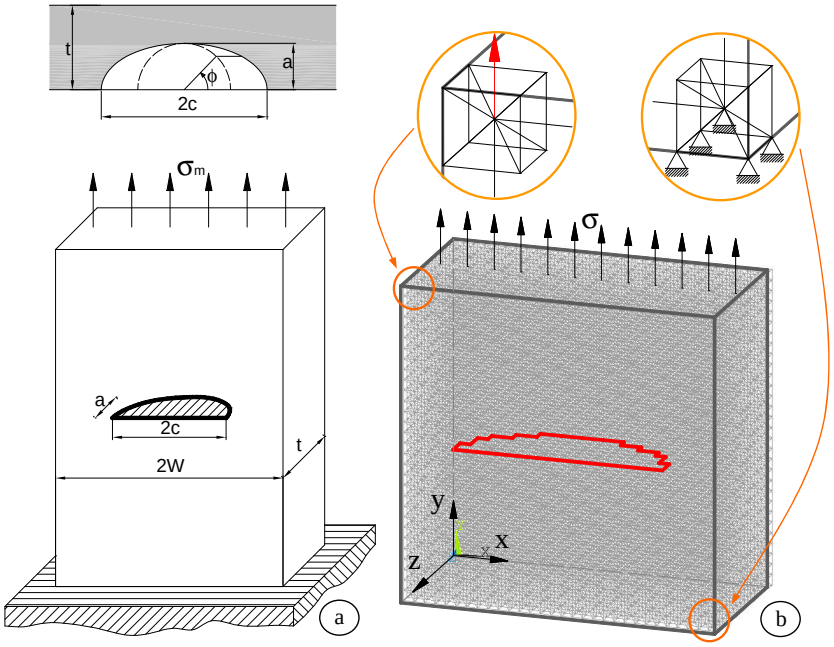

Figure 8 The geometric configuration where the dimensions and boundary conditions details are indicated.

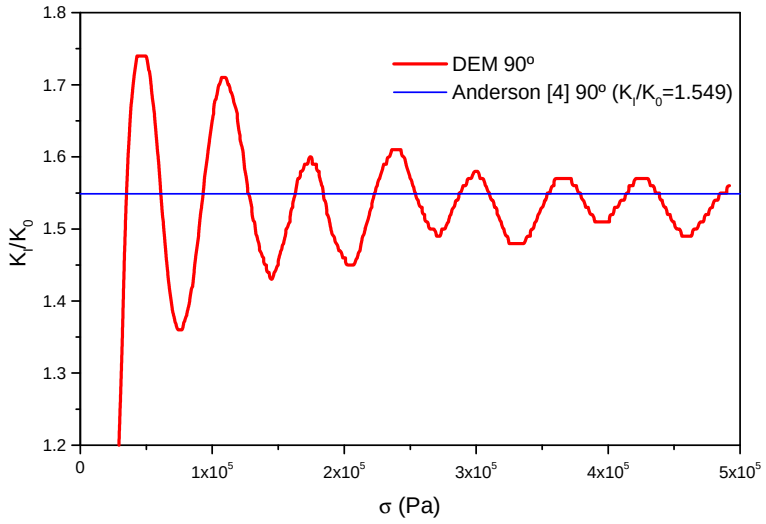

Figure 9 Normalized SIF measure in the direction of the ellipse minor axis vs. applied tensile stress.

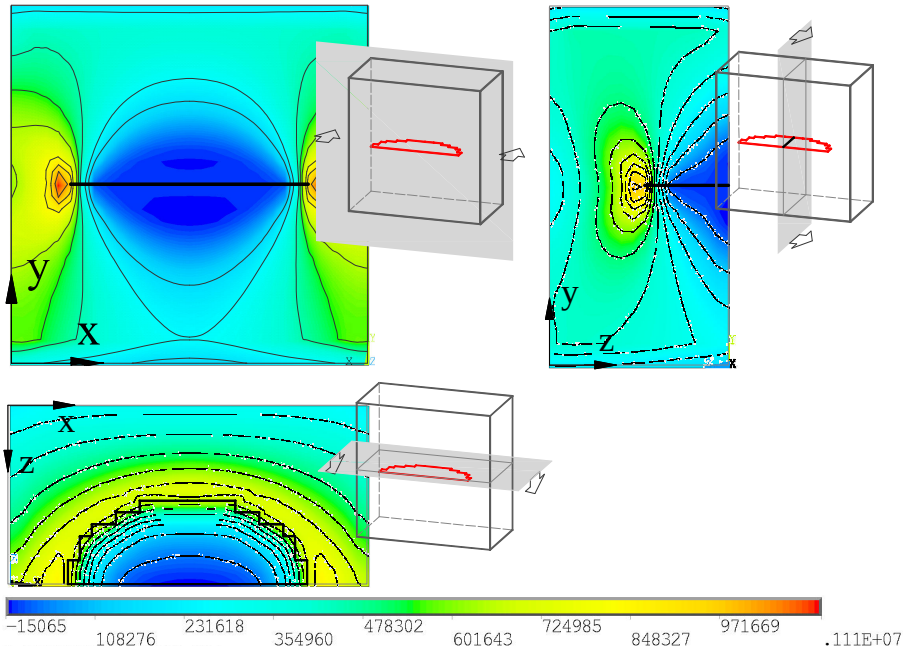

Figure 10 Iso-stress map σ_{yy} (Pa), (a) Frontal view, (b) perpendicular to the crack plane cut, (c) Coincident to the crack plane cut.

In Figure 11 a three-dimensional map of iso-stress σ_{yy} is shown. This figure shows clearly the distribution of stress around the discontinuity.

As it follows, examples in 2 and 3D show where the dynamic SIF was evaluated.

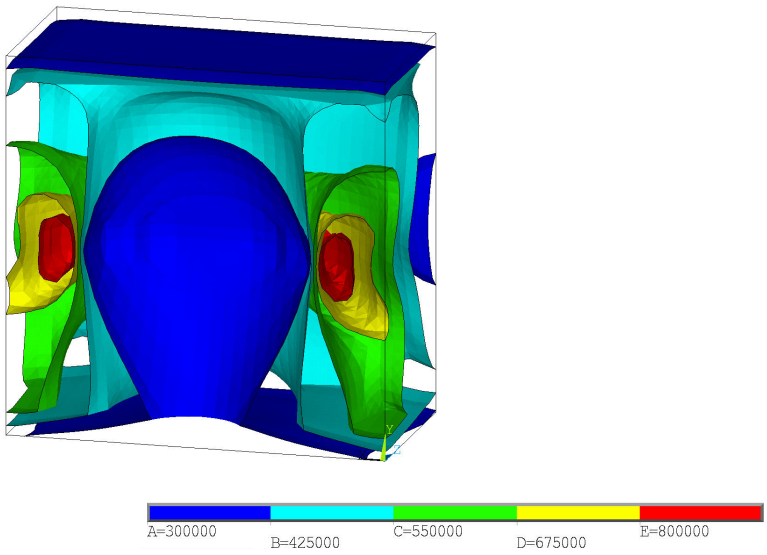

Figure 11 Three-dimensional scheme of the surface of iso-stress σ_{yy} (Pa) in the example 2 (large prismatic block with a plane semi-elliptical crack).

4.3 Example 3: Dynamic SIF calculus for a rectangular plate with a central crack inclined 45°

The present example concerns about the dynamic SIF determination of a rectangular plate with a central crack inclined 45°. It is a problem with a mixed fracture mode, therefore SIF can be decomposed in two characteristic modes (Mode I and II). The plate is dynamically excited in the axial direction following a Heaviside function with the spatial uniform stress from t = 0. The material of the plate is considered elastic linear and its properties are: E =200000 MPa, $\nu = 0.3$, $\rho = 5000$ kg/m^3 and Gc = 300 N/m.

The geometric characteristics of the analyzed problem are shown in Figure 12 (a) and the accomplished discretization with DEM in Figure 12 (b).

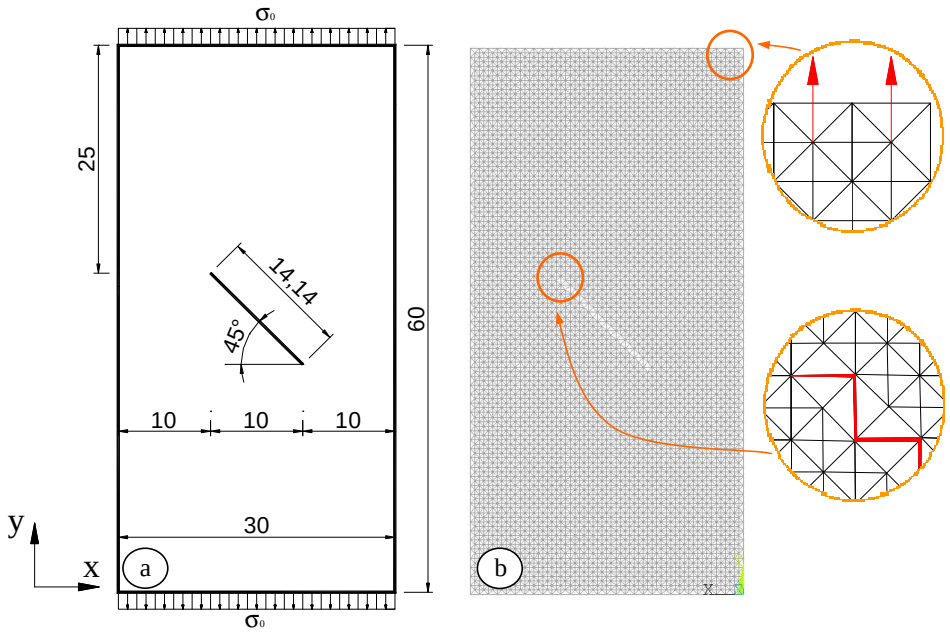

Figure 12 Scheme of the studied plate. (a) geometric characteristics of the cracked plate (dimensions in mm), (b) the DEM model.

4.3.1 DEM Model

The example 3 is modeled through DEM using different types of discretizations. All models have only one module of thickness and the displacements in the perpendicular direction of the plate in all its nodes were restricted to simulate a plane strain condition. Details of how the crack was modeled, doubling its nodes, and how the loads were applied are shown in Fig.12 (b). Table 2 indicates the different discretizations utilized for this analysis, being in all of these: $\nu = 0.25$, and $\Delta t = 1.0\ E^{-8}$ s.

Table 2 Different discretizations and dof utilized for the example 3.

	Lc	Modules	Degrees of freedom
Model A	1.25 E^{-3}m	25 x 49	4784
Model B	1.00 E^{-3}m	31 x 61	7420
Model C	2.50 E^{-4}m	121 x 241	116080
Model D	2.00 E^{-4}m	150 x 300	181100
Model E	1.25 E^{-4}m	241 x 481	462560

4.3.2 Obtained results

Figure 13 a) shows the values of SIF in Mode I and Mode II normalized with $K_0 = (\sigma \cdot \sqrt{\pi \cdot a})$ vs. time, obtained through COD in the context of DEM. In Figure 13 b the results are shown together with the ones from other authors, that is: Dominguez and Gallego [11] that used the BEM in time domain and Krysl and Belytschko [19] that used the Galerkin's method. It is possible to observe that the DEM results have a good correlation with the ones from other authors, taken as reference.

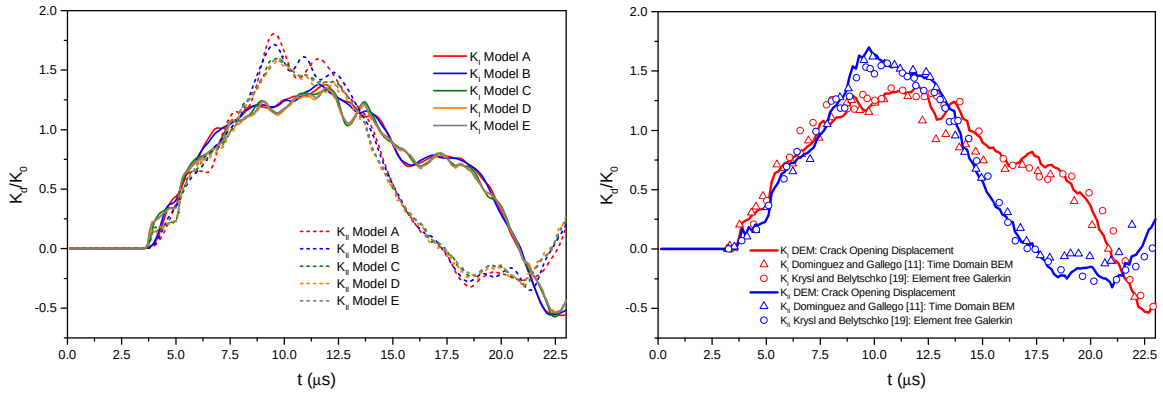

(a) (b)

Figure 13 Results in terms of dynamic normalized SIF for Mode I (K_I) and for Mode II (K_{II}).

The little influence of the discretization is shown in Figure 13 (a) where results A to E models of this example are illustrated.

In Figure 13 b) it can be observed that before the longitudinal wave arrives at the crack tip, that is, when $t < 3.6\mu s$, the SIF value is zero. The maximum SIF value coincides with the time in which the Rayleigh wave, that comes from the farthest border, reaches the crack tip at 9.5 μs.

In Figure 14 a detail of the maximum main stress near the crack tip for a time of 12μs is shown.

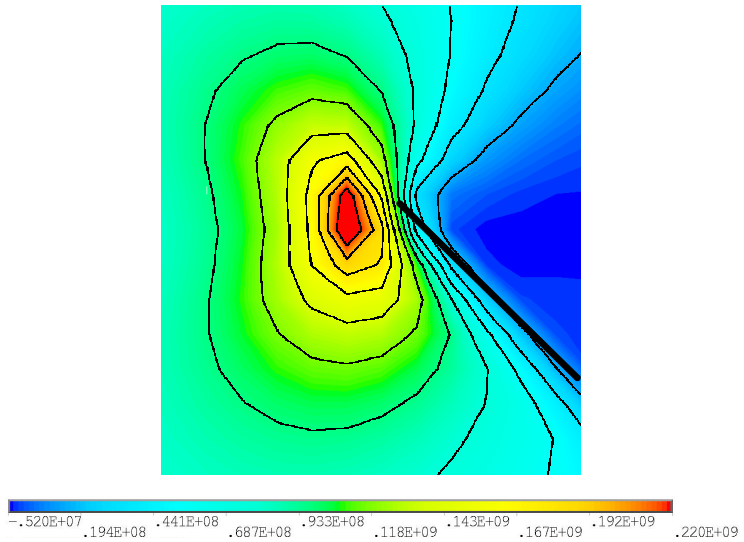

Figure 14 Detail of stress distribution in the crack tip [Pa] in terms of maximum main stress at 12μs.

In Figure 15 a set of graphs that represents the distribution of the maximum main stress on the cracked plate, for different times of the simulated process, is illustrated. It can be observed how DEM captures the behavior of the elastic waves, that in the beginning of the process up to t = 3 μs, move parallel to the border where the external stress was applied.

After t=3.6 μs a stress concentration in both crack tips can be perceived, with maxima values between 12 to 15μs. From this region on the stress in the crack tip begins to decrease following the shape indicated in Figure 15 in terms of normalized SIF.

4.4 Example 4: dynamic SIF calculus for a plate with a border crack inclined 45°

The example 4 corresponds to a rectangular plate with a 45° inclined border crack. In Figure 16 a) its layout is shown. On the plate an external stress is applied with uniform spatial distribution and following a Heaviside time function up to t=0. The material properties are: Shear Modulus 29.4 GPa, the Poisson's ratio 0.286 and the density is 2450 Kg/m^3.

4.4.1 DEM Model

The plate modeled in DEM in the example 4 has 220 elemental modulus of height, 160 modules of width and only one modulus of thickness (it is considered the plane strain condition). In the present case 142072 dof were used taking into account the double nodes in the crack.

In the present example it was necessary to use a very refined discretization to obtain a good accurate result in terms of SIF vs. Time. This problem doesn't present symmetry. For this reason the elastic waves reach the crack in a more complex form and it is mandatory that a more dense discretization than in the previous examples be utilized in order to obtain good results through COD method.

In Table 3 the material properties are shown for the studied example and also the DEM

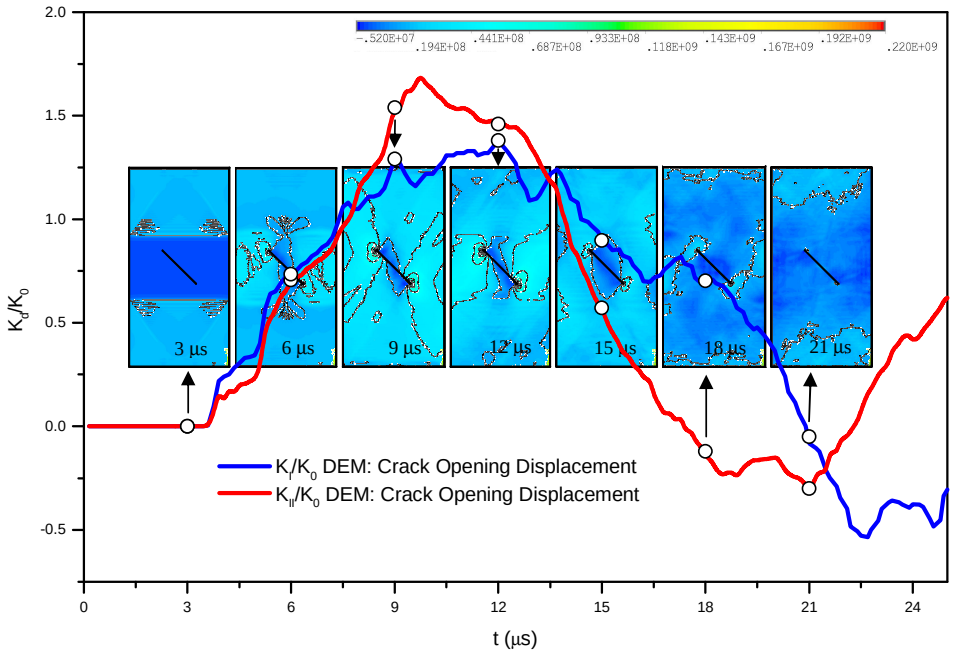

Figure 15 The normalized mode I and II SIF vs. time and the main maximum stress map (Pa) for the example 3.

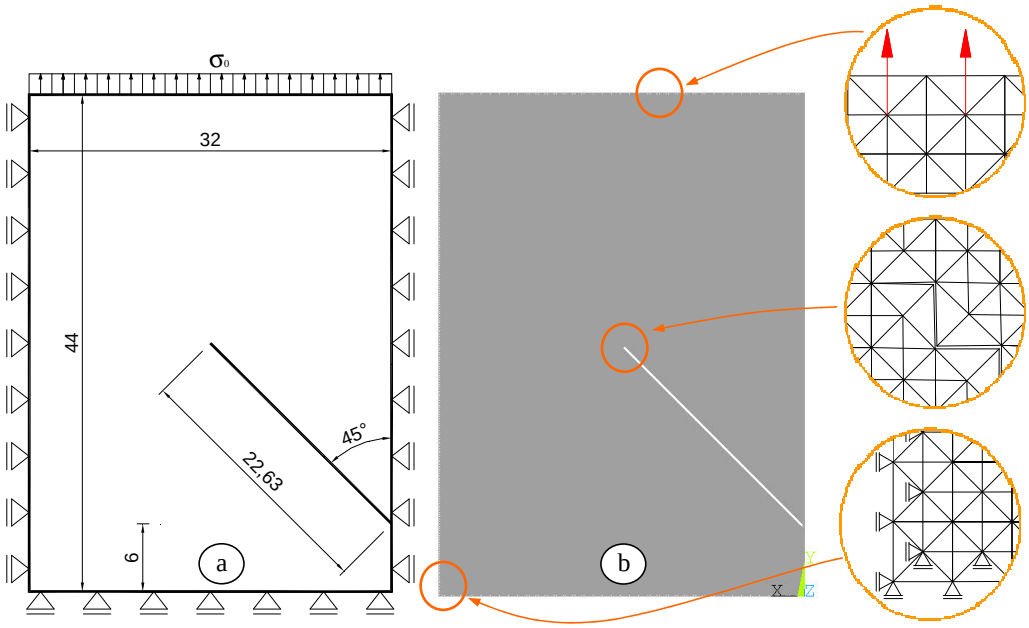

Figure 16 a) Layout of example 4(plate with a inclined border crack)[mm] .b) Model implemented in DEM.

parameters used.

Table 3 Properties of the material for the studied example and DEM parameters used in the present simulation.

Material Properties		DEM Parameters	
E	75.6 GPa	Lc	2.00 E^{-4} m
ν	0.286	ν	0.25
ρ	2450 kg/m^3	Δt	1.0 E^{-8} seg

4.4.2 Obtained results

The curves K_{Id} and K_{IId} vs. time obtained using the COD for the SIF calculus are shown in Figures 17 a) and b) with the results obtained by Dominguez and Gallego [11] who used BEM in the time domain, Kishimoto et al. [17], who applied FEM and by Fedelinsky et al. [12] who used another version of BEM. A good correlation between DEM results and the references can be observed.

The correlation between the elastic wave distribution and the curve SIF vs. time at different times are illustrated in Figure 18. In this Figure it is possible to observe that up to $t_1 = 3.61$ μs, the SIF value is null (where t_1 is the time taken by $\boldsymbol{p}$ wave to reach the crack tip from the border, where the stress was applied).

The interaction between the elastic waves and the boundary conditions characterizes the shape of the K_I, K_{II} vs. time curves.

There is no symmetry in example 4, neither in the geometry configuration nor in the boundary conditions applied on the plate. This situation produces a very complex interaction between the elastic waves that are generated by the applied stress and, despite this, the obtained results with DEM have a very good correlation with the references.

4.5 Example 5: The dynamic SIF for an elliptical crack embedded in a rectangular block

A last example of a dynamic SIF calculus in an elliptical crack embedded in a prismatic block is shown. The body is submitted to a remote axial stress with Heaviside function where time is t>0. Figure 19 presents the geometry and boundary conditions of the model, plus the dimension and the position of the elliptical discontinuity.

The material used was linear elastic considering an elasticity modulus of 200Gpa, and Poisson's ratio of 0.298 and density of 7900 Kg/m^3.

4.5.1 DEM model

The DEM modeled body is composed by 122 modules of height, 72 of width and 48 of thickness. The material properties and the main DEM parameters used in the simulation are summarized in table 4. In the present example 2584809 of dof were necessary to build this model.

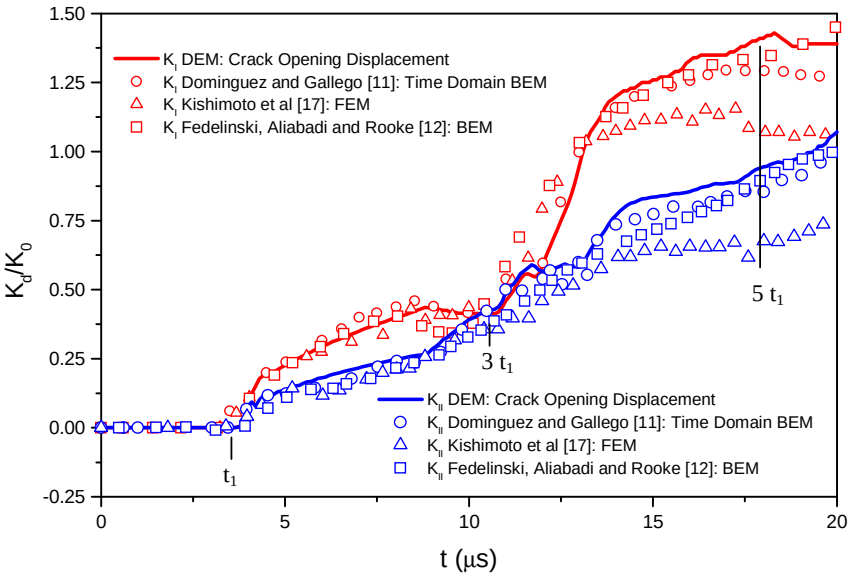

Figure 17 The dynamic normalized Example 4 SIF for the Mode I (K_I) and for the Mode II (K_{II}) .

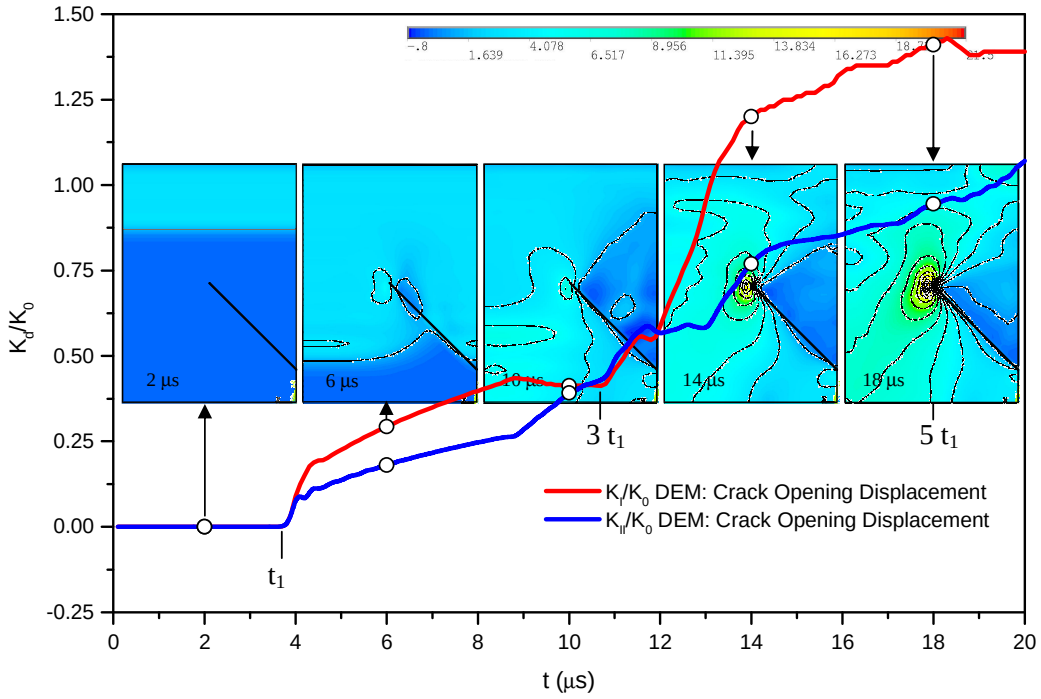

Figure 18 Stress distribution in terms of maximum main stress (Pa) and its relationship with the SIF vs. time curve.

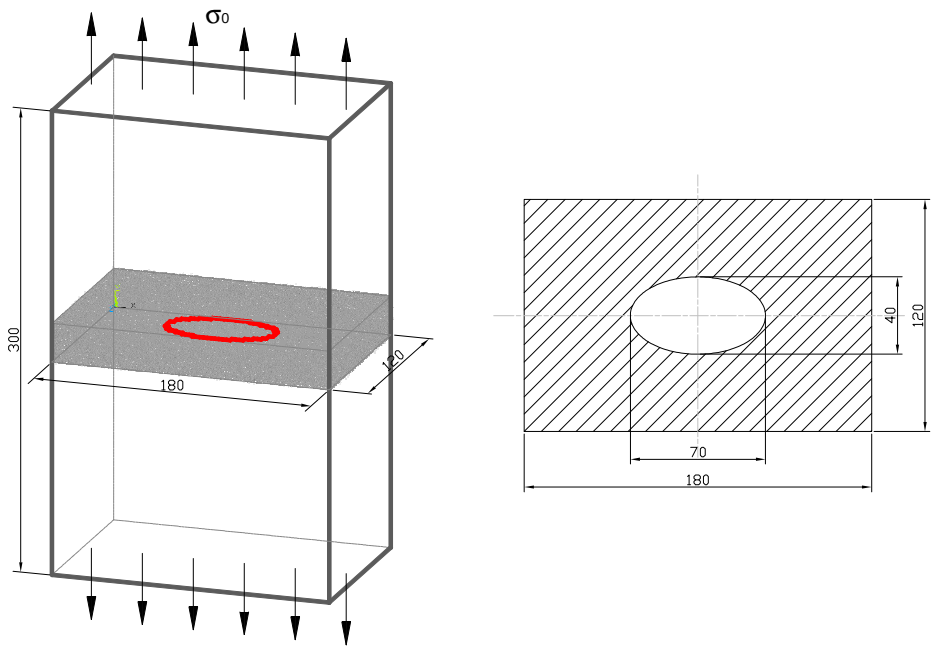

Figure 19 The elliptical crack embedded in a prismatic block, isometric scheme of DEM model, and details of the cracked plane. The dimensions are in mm.

4.5.2 Obtained results

The normalized SIF regarding to the value obtained with equation (4) in the minor axis of the ellipse is shown in Figure 20. In this figure the normalized SIF is graphicated vs. time and compared with other authors' results: Guo and Nairn [13], who used the Material Point Method (MPM); Nishioka [23], the FEM; and Chen and Wilkens [7] the Finite Difference Method (FDM).

Table 4 Material properties and DEM parameters used in the simulation of the Example 5.

Material Properties		DEM Parameters	
E	200 GPa	Lc	2.50 E^{-3} m
ν	0.298	ν	0.25
ρ	7900 kg/m^3	Δt	1.0 E^{-7} seg

As it can be observed from Figure 20 the obtained result with DEM are in correlation with the reference.

In the present example, times that are shorter than $t_1 = 27$ μs, (time in which the elastic waves reach the lips of the elliptical crack), the SIF value is null.

Some waves reflect on the block borders and reach the lips crack at 41 μs. At this time the first peak in the SIF vs. time curve appears (see Figure 20).

Other characteristic point in the SIF vs. time curve of Figure 20 is $t_2 = 47$ μs, that corresponds to the time in which the $\boldsymbol{s}$ waves reach the crack lips. At this time a valley in Figure 20 occurs.

The SIF vs. time curve peak is found when the $\boldsymbol{p}$ waves that reflect in the extreme border parallel to the crack plane reach the lips of the crack at $t_3 = 2$, $t_1 = 54\mu$s, as it is possible to observe in Figure 20. After this point it is too difficult to follow the correlation between the motion elastic waves and the SIF values.

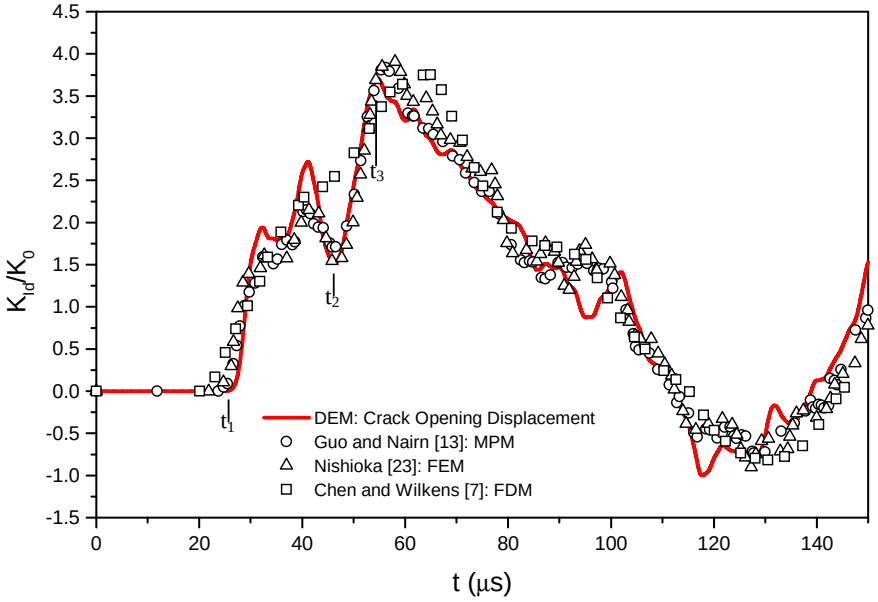

Figure 20 Dynamic SIF normalized by the Mode I (K_I).

5 CONCLUSIONS

In the present work several applications are shown where the static and dynamic SIF for several geometries are calculated in 2 and 3 dimensions. The results shown are compared with other authors' results.

In cases where the dynamic SIF was calculated, the interpretation of SIF vs. time curve was carried out.

During the present work it was possible to conclude that:

– DEM is able to obtain static and dynamic SIF values as it was shown in several examples here presented comparing the DEM results with other results.

In the present paper we do not intend to show DEM as an alternative way to calculate the static and dynamic SIF because DEM has hard restrictions to model complex geometries.

The field in which DEM can be competitive among other classical methods like FEM and BEM is in the simulation of unstable crack propagation and in the simulation of the rupture process in quasi fragile materials.

It is possible to conclude that DEM has the capacity to measure the static and dynamic SIF in 2 and 3 dimensions. And it also lets the stress distribution be captured in all simulated process.

Acknowledgments The authors acknowledge the support of CNPq and CAPES, Brazil, and UNNE, Argentina.

References

[1] E. Absi. Théorie des equivalences-determination de quelques eleménts types. *Anales de L'Institut Technique du Balument el des Travaux Public*, 281(83-86), 1971.

[2] M.H. Aliabadi and D.P. Rooke. *Computational Mechanics Publications*. Kluwer Academic Publishers, The Netherlands, 1991. ISBN 1-85312-057-X.

[3] M.H. Aliabadi and A.L. Saleh. Fracture mechanics analysis of cracking in plain and reinforced concrete using the boundary element method. *Engineering Fracture Mechanics*, 69(2):267–280, 2002.

[4] T.L. Anderson. *Fracture Mechanics. Fundamentals and Applications*. CRC Press, 2005. ISBN: 978-0-8493-1656-2.

[5] R.G. Batista. Aplicao do método dos elementos discretos ao estudo de micromecanica do dano de materiais microporosos de matriz metálica. dissertação (doutorado). Technical report, Programa de posgraduação em engenharia mecânica da UFRGS, Universidade Federal do Rio Grande do Sul, 2007.

[6] A. Brara, F. Camborde, J.R. Klepaczko, and C. Mariotti. Experimental and numerical study of concrete at high strain rates in tension. *Mechanics of Material*, 33:33–45, 2001.

[7] Y.M. Chen and M.L. Wilkens. Numerical analysis of dynamic crack problems. In *Elastodynamic Crack Problems*, pages 317–325, The Netherlands, 1977. Noordhoff International Publishing.

[8] P.A. Cundall and R.D. Hart. Numerical modelling of discontinua. In *Proceedings of the 1st U.S. Conference on Discrete Element Methods*, pages 1–17, Golden, Colorado, 1989.

[9] P.A. Cundall and O.D.L. Strack. A discrete numerical model for granular assemblies. *Géotechnique*, 29(1):47–65, 1979.

[10] A. Dalguer, K. Irikura, and J.D. Riera. Generations of new cracks accompanied by dynamic shear rupture propagation of the 2000 tottori (japan) earthquake. *Bulletin of the Seismological Society of America*, 93:2236–2252, 2003.

[11] J. Dominguez and R. Gallego. Time domain boundary element method for dynamic stress intensity factor computations. *Int. J. Num. Meth. Engng*, 33:635–647, 1992.

[12] P. Fedelinski, M.H. Aliabadi, and D.P. Rooke. The dual boundary element method in dynamic fracture mechanics. *Engineering Analysis with Boundary Elements*, 12:203–210, 1993.

[13] Y.J. Guo and J.A. Nairn. Three-dimensional dynamic fracture analysis using the meterial point method. *Tech Science Press, CMES*, 1(1):11–25, 2006.

[14] Y. Hayashi. Sobre um modelo de discretização de estruturas tridimensionais aplicado em dinâmica não linear. Master's thesis, Curso de Pós-Graduação em Engenharia Civilem Engenharia Civil, Universidade Federal do Rio Grande do Sul, Porto Alegre, 1982.

[15] A. Hrenikoff. Solution of problems of elasticity by the framework method. *Journal of Applied Mechanics*, 12:169–175, 1941.

[16] I. Iturrioz, L. Miguel, and J.D. Riera. Dynamic fracture analysis of concrete or rock plates by means of the discrete element method. *Latin American Journal of Solids and Structures*, 6(3):229–245, 2009.

[17] K. Kishimoto, S. Aoki, and M. Sakata. Dynamic stress intensity factors using J-integral and finite element method. *Engineering Fracture Mechanics*, 13(2):387–394, 1980.

[18] L. Kosteski, R. Barrios, and I. Iturrioz. Determinación de parámetros fractomecánicos estáticos y dinámicos utilizando el método de los elementos discretos compuestos por barras. *Revista Internacional Métodos numéricos para cálculo y diseño en ingeniería, Cimne*, 24(4):323–343, 2008.

[19] P. Krysl and T. Belytschko. The element free Galerkin method for dynamic propagation of arbitrary 3D cracks. *International Journal for Numerical Methods in Engineering*, 154:133–150, 1999.

[20] L.F.F. Miguel, J.D. Riera, and I. Iturrioz. Influence of size on the constitutive equations of concrete or rock dowels. *International Journal for Numerical and Analytical Methods in Geomechanics*, 32(15):1857–1881, 2008.

[21] A. Munjiza, T. Bangash, and N.W.M. John. The combined Finite-Discrete Element Method for structura failure and collapse. *Engineering Fracture Mechanics*, 71:469–483, 2004.

[22] A.A. Needleman. Continuum model for void nucleation by inclusion debonding. *Journal of Applied Mechanics*, 54:525–531, 1987.

[23] T. Nishioka. Recent developments in computational dynamic fracture mechanics. In *Dynamic Fracture Mechanics*, pages 1–58, Southampton, UK, 1995. Computational Mechanics Publications.

[24] T. Nishioka. *Fracture a Topical Encyclopedia of Current Knowledge. Chapter 30, Edited by G. P. Cherepanov.* Krieger Publishing Company, Malabar Florida, 1998.

[25] J.D. Riera and I. Iturrioz. Discrete element dynamic response of elastoplastic shells subjected to impulsive loading. *Communications in Num. Meth. in Eng.*, 11:417–426, 1995.

[26] J.D. Riera and I. Iturrioz. Discrete element model for evaluating impact and impulsive response of reinforced concrete plates and shells subjected to impulsive loading. *Nuclear Engineering and Design, Elsevier*, 179:135–144, 1998.

[27] R.D. Rios and J.D. Riera. Size effects in the analysis of reinforced concrete structures. *Engineering Structures*, 26:1115–1125, 2004.

[28] D.P. Rooke and D.J. Cartwright. The compendium of stress intensity factors. *Her majesty's Stationery Office*, 1976.

[29] F. Schnaid, L. Spinelli, I. Iturrioz, and M. Rocha. Fracture mechanics in ground improvement design. *Ground Improvement*, 8:7–15, 2004.

[30] A. Tabiei and J. Wu. Development of the dyna3d simulation code with automated fracture procedure for brick elements. *International Journal for Numerical Methods in Engineering*, 57:000–000, 2003. DOI: 10.1002/nme.742.

[31] T.W. Tech, R.G. Batista, I. Iturrioz, and A. Cisilino. Aplicação do m'etodo dos elementos discretos em mecânica de fratura estática e dinâmica. In *XXV Iberian Latin-American Congress on Computacional Methods in Engineering*, Recife, 2004.

[32] P.H. Wen, M.H. Aliabadi, and D.P. Rooke. Cracks in three dimensions: A dynamic dual boundary element analysis. *Computer methods in applied mechanics and engineering*, 167:139–151, 1998.